

Hydrodynamic simulation of an oscillating hydrofoil near free surface in critical unsteady parameter



Esmaeil Esmaeilifar^a, Mohammad Hassan Djavareshkian^{a,*}, Behzad Forouzi Feshalami^a, Ali Esmaeili^b

^a Department of Mechanical Engineering, Ferdowsi University of Mashhad, Iran

^b Instituto Superior Técnico, Universidade de Lisboa, Portugal

ARTICLE INFO

Keywords:

Plunging hydrofoil
Free Surface
Critical Unsteady Parameter
Submergence depth
CFD

ABSTRACT

In this research study, unsteady, viscous and turbulent fluid flow around a plunging hydrofoil is simulated near the water free surface for different submergence depths and oscillation frequencies. The Navier-Stokes (N-S) equations are discretized by employing the finite volume method (FVM) and are solved by using the Pimple algorithm. The volume of fluid (VOF) technique is applied to capture the free surface. To validate the present simulations, a part of the results is compared with experimental results. The aim of the current study is to clarify the physics of flow in the critical unsteady parameter range. Furthermore, the effects of free surface and surface waves on hydrofoil drag are analyzed. Moreover, instantaneous drag behavior, the shape of the surface waves and the effect of the free surface on trailing edge vortices (TEV) are investigated at subcritical, supercritical and especially near critical Strouhal number. The results demonstrate that the main reason behind the sudden drag increment in the critical unsteady parameter is the generated powerful waves in this region which transfer more momentum and finally lead to drag increment. In addition, the free surface affects TEV and causes drag increment at all frequencies at the submergence depth of $0.5c$ and critical frequency of other depths. However, the free surface does not have any effects on the vortices in other cases.

1. Introduction

Hydro-crafts have been attended in recent years due to their ability. The most important goal of designing this vehicle is to achieve maximum velocity and simultaneously reduce wasted energy to a minimum which would lead to a reduction in greenhouse gasses and carbon dioxide emissions. Thus, attaining these aims needs the application of some of the techniques to decrease drag and also increase thrust force. One of these techniques is to inject micro-bubbles (McCORMICK and Bhattacharyya, 1973; Shen et al., 2006) and polymers (Winkel et al., 2009) into the surface boundary layer. However, this method is only suitable for low velocities. Separation of air and gas leads to significant drag increment in unsteady flows (Ceccio, 2010). Another technique to reduce the drag is utilizing hydrofoils under the boat's hull. This technique can create a lift force that will subsequently cause detachment of the boat's body from the water surface which finally leads to drag decrement. Therefore, many studies have been conducted in order to improve hydrofoil performance and efficiency (Djavareshkian and Esmaeili, 2013, 2014; Djavareshkian et al., 2013; Ducoin et al., 2009; Kim and Yamato,

2005; Kouh et al., 2002; Münch et al., 2010; Xie and Vassalos, 2007; Zanette et al., 2010). Undergoing plunging motion is another advantage of hydrofoils due to the influence of ocean waves on hydro-crafts. Therefore, when the hydro-craft moves forward, the plunging motion of hydrofoil produces a thrust force which can reinforce the propulsion of the hydro-craft. Nevertheless, Prasad et al. (2015) simulated a stationary hydrofoil to investigate the free surface impact on wave profiles, pressure contour, lift and drag coefficients at various submergence depths. As expected, the obtained results cannot be accurate. The drag of oscillating foil is less than the stationary one due to experiencing unsteady aerodynamic properly according to the Knoller-Betz effect. In other words, the vertical movement of oscillating foils creates an effective angle of attack. Subsequently, a vertical force is created in the direction of this angle with lift and thrust force components. This process is known as the Knoller-Betz effect (Jones et al., 1998). Owing to this point, Chung (2016) used a flapping plate to study the impacts of changing Froude number, normalized submergence depth on the time-averaged thrust coefficient and the propulsive efficiency in the vicinity of the surface at $Re=1000$. The vortices pattern created at the foil trailing edge can generate drag or thrust force. It

* Correspondence to: P.O.B. 9177948944 Mashhad, Iran.

E-mail address: jarareshkian@um.ac.ir (M. Hassan Djavareshkian).

Nomenclature

C	Chord length (m)
2D	Two dimension
d	Submergence depth
FVM	Finite volume method
LRN	Low Reynolds Number
N-S	Navier-Stokes equations
P	Pressure

Re	Reynolds number
$Fr = \frac{U_0}{\sqrt{g_c}}$	Froude number
$Sr_c = \frac{fc}{U_0}$	Strouhal number (based on chord length)
TEV	Trailing edge vortices
U_0	Free stream velocity
VOF	Volume of fluid
C_{LF}	Longitudinal force coefficient
ρ	Density (kgm^{-3})

should be noted that the pattern with clockwise vortices on the upper row and counter-clockwise on the lower row produces drag. This pattern can be reversed by increasing the frequency or foil amplitude which can finally result in thrust generation due to momentum increment (Jones et al., 1998; Young and Lai, 2004). Moreover, Cleaver et al. (2014) and Cleaver et al. (2016) experimentally verified that using oscillating flexible wing and foil can reverse the mentioned pattern and lead to lift and thrust increment, respectively. Actually by this work, they connected unsteady aerodynamic to flexible structures. An important challenge to design hydrofoils is the situation in which they are constrained to move in the vicinity of the water free surface due to the significant impact of this surface and ocean waves on their performance. In other words, Proximity to the surface led to a decrease in drag reduction (Cleaver et al., 2013). Many researchers, Hough and Moran (1969), Plotkin (1975), Xu and Wu (2013), have analyzed the effects of linear free surface on hydrodynamic simulation of submergence hydrofoil. However, because of the non-linear inherency of the free surface, precise results are not acquired. Therefore, Forbes (1985), Bai and Han (1994) and Landrini et al. (1999) have studied non-linear free surface effects on hydrofoils. The free surface causes drag increment of foil especially in the critical unsteady parameter range where large unsteady waves are created (Grue et al., 1988). Potential flow and green function have been applied in many research studies in a range of critical unsteady parameters (Filippas and Belibassakis, 2014; Haskind, 1954; Xu and Meng, 2016). However, the problem converts to a linear one due to the assumption of inviscid flow, and the results do not have enough accuracy. As Dagan and Miloh (1982) and Palm and Grue (1999) have discussed, velocity potential function is infinity in critical unsteady parameter and the waves with infinity domain will be produced. In other words, resonance will happen. In contrast with potential flow results, this resonance is not physical and has not been seen in experimental studies. Zhu et al. (2006) applied boundary element method and spectral technique to simulate three dimensional flows around oscillating foil near the free surface. Their results indicated that the produced waves in free surface can be divided into three parts: the first is Kelvin steady waves of forward motion; the second is unsteady waves of foil oscillating motion and the last one is the waves of TEV. The simulation was conducted in a vast range of unsteady parameters with a focus on the critical one. De Silva and Yamaguchi (2012) investigated the possibility of energy extraction from gravitational waves by 2D oscillating hydrofoil near the free surface. The effective parameters were analyzed on the thrust force of hydrofoil with pitching and plunging motion. However, their study was not in a range of critical unsteady parameters and also the physics of flow was not discussed. In addition to analytical and computational studies, an experimental investigation has been conducted by Cleaver et al. (2013). They experimentally studied the influences of amplitude and submergence depth on drag reduction of oscillating hydrofoil in a large range of oscillation frequencies. Based on their research, reduction of produced thrust force by reducing submergence depth is significant in critical unsteady parameter. Particle Image Velocimetry was utilized to clear more details around the oscillating hydrofoil to assess the main reason behind the alteration in critical unsteady parameter range. However, accurate and wide detection of flow is not

possible in experimental research even by utilizing the most advanced techniques. However, numerical computer simulation can present accurate details of flow. CFD methods are applied in many numerical research studies due to their accuracy. Furthermore, the results of CFD methods for submergence hydrofoil in unsteady, viscous flow have had acceptable agreement in comparison with experimental data (Prasad et al., 2015).

To summarize, in order to simulate oscillating hydrofoil in the vicinity of the water surface accurately, we should avoid eliminating the free surface impact. Additionally, using fixed hydrofoil or inviscid flow for simplicity leads to inaccurate results. However, taking into account the mentioned factors add complexities to the simulation. Thus, most of the mentioned numerical studies have ignored these points and the others without these assumptions have focused on modeling other bodies. Therefore, plunging hydrofoil in unsteady, viscous and turbulent flow is numerically investigated by consideration of free surface impacts in this paper. The N-S equations are discretized by FVM and are solved by using the PIMPLE algorithm (Jasak, 1996). Considering the results obtained, the N-S equations properly dealt with the infinity content problem of the velocity potential function in the critical unsteady parameter. The aim of the current study is to clarify the physics of flow in plunging motion near the free surface in the critical unsteady parameter range. Furthermore, the effects of free surface and surface waves on hydrofoil drag are analyzed separately. Moreover, instantaneous drag behaviors, the shape of surface waves, the effect of the free surface on TEV are investigated in the subcritical, supercritical and especially near critical Strouhal number.

2. Problem description and the governing equations

A 2-D NACA0012 hydrofoil with a chord length of C which is submerged at a distance of d from the free surface of water and air as shown in Fig. 1 is investigated in this research study. Uniform free stream with velocity of U_0 passes through the hydrofoil in the x-direction and simultaneously plunging oscillating motion is applied to the hydrofoil by equation 1.

$$y = a \sin \omega t \quad (1)$$

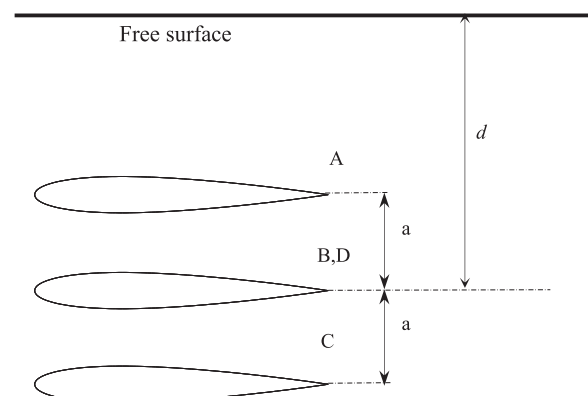


Fig. 1. General schematics of problem and plunging motion.

In this equation, a is the amplitude of plunging motion, ω is angular frequency and t is the time. Four phases of different plunging motions are defined by A, B, C and D which denote the upper zone, the middle zone downward, the lower zone and middle zone upward, respectively. The variable parameters of amplitude and submergence depth are used in dimensionless form. Here g, ω and U_0 are gravitational acceleration, angular frequency of plunging motion and free stream velocity respectively. These are the important parameters of an oscillating hydrofoil in the vicinity of the water free surface. Thus, unsteady parameter $\tau = \omega U_0/g$ has a significant role to analyze this problem. It is important to consider the unsteady parameter of 0.25 as the critical one. In subcritical unsteady parameter, four surface gravitational waves will be formed three of which are propagated downstream and the other one is propagated upstream. By increasing the oscillation frequency in order to convert unsteady parameter to a critical one, the group velocity of wave 1 which moves to the upstream was decreased and achieves free stream velocity as indicated in Fig. 2. Additionally, the group velocity of wave 2 which moves downstream was increased and it will be equal to the free stream velocity. Finally these two waves will be eliminated. Note that the analytical relations to compute these waves velocity are mentioned by Grue et al. (1988). It should be noted that no upstream wave can propagate in supercritical frequency since information wave velocity is less than the free stream velocity in this condition. In this research, the physics of flow is studied numerically with a focus on critical unsteady parameter. Continuity and momentum equations are as follows:

$$\frac{\partial u}{\partial x} + \frac{\partial v}{\partial y} = 0 \tag{2}$$

$$\frac{\partial u}{\partial t} + u \frac{\partial u}{\partial x} + v \frac{\partial u}{\partial y} = -\frac{1}{\rho} \frac{\partial p}{\partial x} + \nu \left(\frac{\partial^2 u}{\partial x^2} + \frac{\partial^2 u}{\partial y^2} \right) \tag{3}$$

$$\frac{\partial v}{\partial t} + u \frac{\partial v}{\partial x} + v \frac{\partial v}{\partial y} = g - \frac{1}{\rho} \frac{\partial p}{\partial y} + \nu \left(\frac{\partial^2 v}{\partial x^2} + \frac{\partial^2 v}{\partial y^2} \right) \tag{4}$$

Where $U = ui + vj$ is the fluid velocity vector, u and v are the x-component and y-component of velocity vector. The SST $k - \omega$ model (Menter, 1994) is used to simulate the turbulence nature of flow. This turbulence model uses $k - \omega$ standard model for the inner part of the boundary layer. So no more relaxation factor is needed to use as turbulent model of low Re. The $k - \epsilon$ Standard model is applied for the outer part which does not have the sensitivity problem of the $k - \omega$ model to free stream at entrance. The turbulence kinetic energy and specific dissipation rate equations are as follows:

$$\frac{\partial k_t}{\partial t} + U_j \frac{\partial k_t}{\partial x_j} = P_k - \beta^* k_t \omega_t + \frac{\partial}{\partial x_j} \left[(\nu + \sigma_k \nu_t) \frac{\partial k_t}{\partial x_j} \right] \tag{5}$$

$$\begin{aligned} \frac{\partial \omega_t}{\partial t} + U_j \frac{\partial \omega_t}{\partial x_j} = & \alpha S^2 - \beta \omega_t^2 + \frac{\partial}{\partial x_j} \left[(\nu + \sigma_\omega \nu_t) \frac{\partial \omega_t}{\partial x_j} \right] \\ & + 2(1 - F_1) \sigma_{\omega 2} \frac{1}{\omega_t} \frac{\partial k_t}{\partial x_j} \frac{\partial \omega_t}{\partial x_j} \end{aligned} \tag{6}$$

Where k_t and ω_t are turbulence kinetic energy and specific dissipation rate, respectively. $P_k, \beta^*, \alpha, \beta, S, \sigma_\omega, F_1, \sigma_{\omega 2}$ are defined as in (Menter, 1994). Furthermore, U_j is the velocity, ν is the kinematic viscosity, ν_t is the eddy viscosity and x_j is the position.

The VOF method is used to simulate two-phase flow and capture the free surface between water and air. The VOF function is defined owing to solving its scalar transition equation. Thus, the volume fraction ratio of each fluid phase will be obtained for each cell and moment (Hirt and Nichols, 1981).

$$\frac{\partial F}{\partial t} + u \frac{\partial F}{\partial x} + v \frac{\partial F}{\partial y} = 0 \tag{7}$$

When $F = 0$ and 1, the cell is full of air and water, respectively. Also

$0 < F < 1$ denotes the cells with some water and some air. Free surfaces are formed by this cells.

3. Numerical modeling

3.1. Mesh and solver

In this simulation, the fully structured mesh is developed. Due to the significant decrement of the H-type mesh quality around the hydrofoil, the C-type mesh is utilized in this region. However, the C-type mesh cannot efficiently simulate the produced waves in the free surface due to the presence of free surface and geometrical shape of the computational domain because the mesh should be fully orthogonal around the free surface and tiny enough in the y-direction. Thus, the H-type mesh is used in order to capture the free surface carefully for the other computational domain (Fig. 3). The height of the first cell on the hydrofoil surface is 0.004 of chord length which leads to Y_{plus} less than 5 and there are 83 cells on the surface of the hydrofoil in the x direction. In this condition, the first cell is located in the substrate of the boundary layer where the flow can be considered laminar and stress relation can be utilized to compute stresses on the wall. Furthermore, the height of the first cell on the free surface is 0.004 of chord length which is tiny enough to capture surface waves efficiently.

An unsteady multiphase solver called InterDyMFOAM which is available in the open source software, OPENFOAM 2.3 is employed to model the flow and solve the N-S equation. This solver handles dynamic meshes and uses the VOF method to capture the free surface. Dynamic mesh is used to handle moving-body simulation and grid is modified instantly according to the boundary movement. Linear tension spring technique (Gnoffo, 1982) is used in dynamic grids to model variation of movements in boundaries. In this method, which is the most common method to move the volume mesh, each edge between two nodes of the grid, is virtually converted to a spring, where stiffness is proportional to inverse of distance between the nodes, in a way that lines with longer length have lower stiffness and lines with shorter length have higher stiffness. In the present study, this technique is used in order to investigate plunging motion of the hydrofoil. The SST $k - \omega$ model is considered to simulate turbulent flow. Convection terms are discretized by second order scheme with restrictive feature. Owing to the existence of the free surface, the flow is very unstable in the vicinity of the free surface. Thus, choosing the one order scheme keeps the stability of solving stability but its accuracy will be affected significantly. Therefore, a bounded second-order scheme guarantees both solving stability and accuracy. The terms of time and VOF equation are discretized by the second-order scheme of Van leer and the one order scheme of Euler, respectively. The PIMPLE hybrid algorithm that is a combination of SIMPLE and PISO algorithms is used to solve the pressure-velocity coupling equations. The results have verified its ability to preserve solving stability in high courant number.

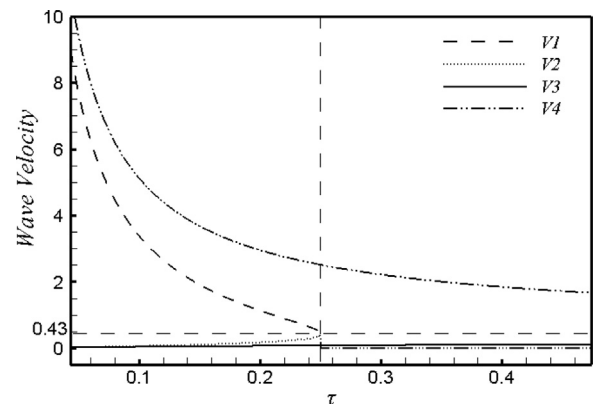


Fig. 2. Group velocity of surface waves.

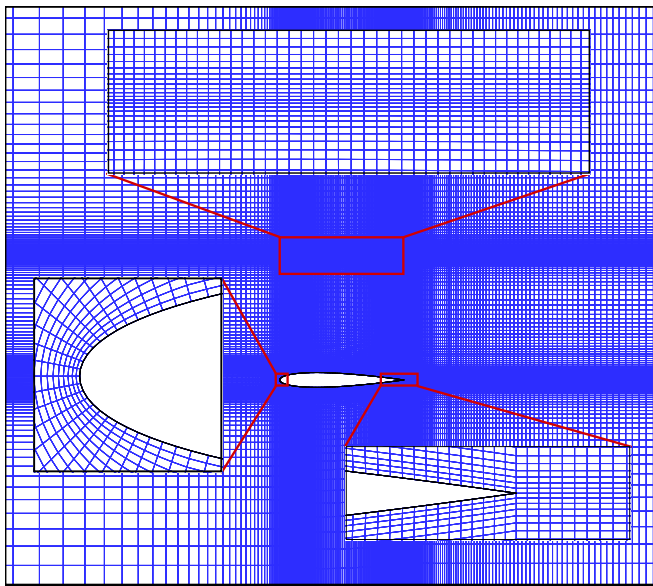


Fig. 3. Mesh resolution around hydrofoil and free surface.

3.2. Computational domain and boundary conditions

The computational domain in the downstream should be large enough in order to prevent reflection of waves at computational domain termination and also due to the formation of surface waves by hydrofoil oscillation in the far field. The thrust force on the hydrofoil and the waves composed in the downstream of the computational domain are investigated with the length of $25c$, $40c$ and $60c$. The results implied that the length of $40c$ is the best option to apply for the downstream of the computational domain. Constant velocity and constant pressure are considered for entrance and exit boundary conditions, respectively. Besides, slip type boundary condition is assumed for the upper and lower boundaries. In addition, the hydrofoil surface is considered as wall.

3.3. Mesh independency study and unsteady convergence

Three different meshes with the same approach in mesh production are picked out to study mesh independency. The length of mesh elements is reduced by a constant ratio using a principled method. In other words, the number of cells of all edges is increased by the ratio of 1.2, and thus grids that consist of 43000, 59000 and 85000 cells are generated. Mean content of thrust force and instantaneous thrust coefficient figures for these grids are represented in Table 1 and Fig. 4 respectively. By comparing the obtained results with those of Cleaver et al. (2013), the mesh with 59000 cells is chosen.

Solution convergence analysis in unsteady flow is different from that of steady flow. So convergence should be investigated in each time step. Furthermore, iteration number is directly related to the number of the time step. In other words, when the iteration number increases in each level, a larger time step can be selected. Four different time steps are tested by dividing the oscillation period of the plunging hydrofoil (T) to 500, 750, 1000 and 2000 in order to choose the best one. By comparing the mean thrust force in each time step and the experimental data of Cleaver et al. (2013), $T/1000$ is chosen for simulation. Additionally, amplitude and oscillation frequency are considered in order to make the flow periodic. In other words, the thrust force produced by plunging motion increases by increasing Strouhal number based on amplitude (St_A) which is combination of oscillation frequency and amplitude. However, periodic behavior of flow converts to a non-periodic one after a specified point which makes stability and body control difficult. The effects of amplitude and

oscillation frequency on periodicity and repeatability of plunging motion cycles were studied numerically by Ashraf et al. (2012). The ranges of amplitudes and oscillation frequencies in which the flow behavior were periodic and non-periodic were determined. The results indicated that the samples analyzed were in a range of periodic flows. Subsequently, the flow behavior, especially the instantaneous thrust force of the oscillating hydrofoil, would have periodic after a few cycles. Due to the simulation process, iteration number of oscillation cycles is chosen such that the flow is periodic. For instance, the mean thrust force diagram for thirty three oscillation cycles is demonstrated in Fig. 5 at $St_c = 0.1$ and $d = c$.

4. Validation

In order to validate the obtained results of this research, contents of mean thrust force for a variety of unsteady parameters (Fig. 6) and also free surface shape (Fig. 7) are compared with the experimental data reported by Cleaver et al. (2013). Geometrical parameters and flow conditions of this experimental study are listed in Table 2. It is important to note that variable of the vertical axis in the mentioned diagrams is the difference of mean thrust force of one temporal cycle from stationary hydrofoil drag. Furthermore numerical results of drag and lift coefficient as a function of angle of incidence is compared with experimental data (Custodio et al., 2015) in Fig. 8 and Fig. 9.

As it is shown in the Figures, the thrust force is reduced significantly in the critical unsteady parameter range, and this physical phenomenon is captured by the numerical solver as well. The maximum difference between the mean thrust force in the present research work and that of experimental data is 6.65%.

5. Results

In this paper, an oscillating hydrofoil is simulated in the vicinity of the water surface. The results are reported for four different submergence depths for a large range of frequencies. The surface effect is not considered for the first case in which hydrofoil is located at an infinite distance from the surface. For the other three cases, the submergence depth is set to $0.5c$, c and $2.25c$.

At first, the impact of oscillation frequency on the thrust force is evaluated as shown in Fig. 10. It is observed that by an increase in frequency, the produced thrust force increases. For this hydrofoil in non-critical frequency and the vicinity of the surface, the behavior of the forces is approximately similar to that of infinite submergence depth. As demonstrated in Fig. 10 and mentioned by Grue et al. (1988), the thrust force produced in the vicinity of the water is affected by two factors. The first one is the mean transferred momentum of TEV and the other one is the transferred momentum by surface waves. This transferred momentum can increase or decrease the mean thrust force due to wave properties and propagation direction. A dimensionless velocity profile for oscillating hydrofoil is provided in Fig. 11 at $t = T/2$. In this Figure, the velocity profile is represented for $d/c = \text{inf}$ and $d/c = 0.5$. Obviously, for $d/c = \text{inf}$, only the vortices produced at the trailing edge can transfer momentum. However, surface gravitational waves can transfer momentum under other conditions too. There is a significant difference in propagation of surface waves in subcritical and supercritical unsteady parameters. Therefore, the flow regime can be

Table 1
Mesh independency results.

Mesh	Mean thrust force coefficient	Difference from the tiniest mesh (%)
85000 cells	0.0158526	0%
59000 cells	-0.0158507	0.01%
43000 cells	-0.0184248	16%

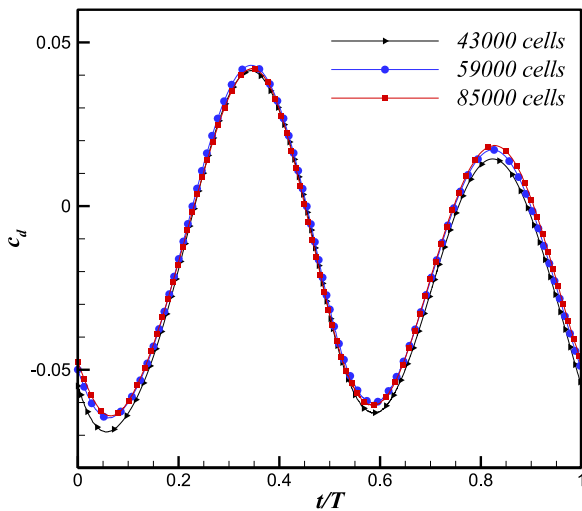


Fig. 4. Mesh independency results.

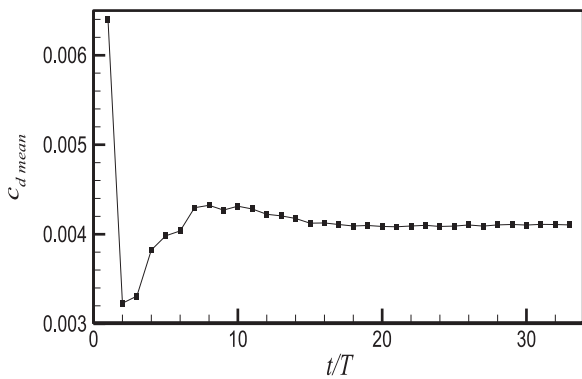


Fig. 5. Mean drag coefficient at $Sr_c = 0.1$ and $d/c = 1$.

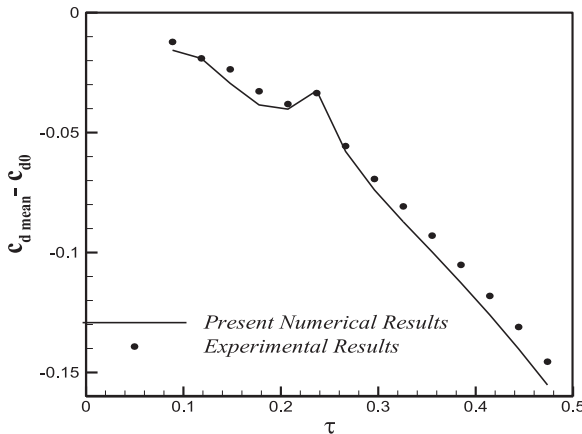


Fig. 6. Validation of numerical results with experimental data of Cleaver et al. (2013).

divided into unsteady parameters of subcritical, and supercritical regions in order to clarify flow physics and mechanism of thrust force production. Furthermore, the results obtained for four different submergence depths are compared for the mentioned parameters. In addition to oscillation frequency, submergence depth is an effective parameter on hydrofoil behavior. The influence of submergence depth on thrust force is investigated for different unsteady parameters.

Generally, by the thrust force increases when there is an increase in frequency and subsequently there is an increase in the unsteady parameter. For this hydrofoil in the vicinity of the surface and non-critical unsteady parameter, behavior of the forces is almost similar to that of infinitive submergence depth. The maximum effect of the free

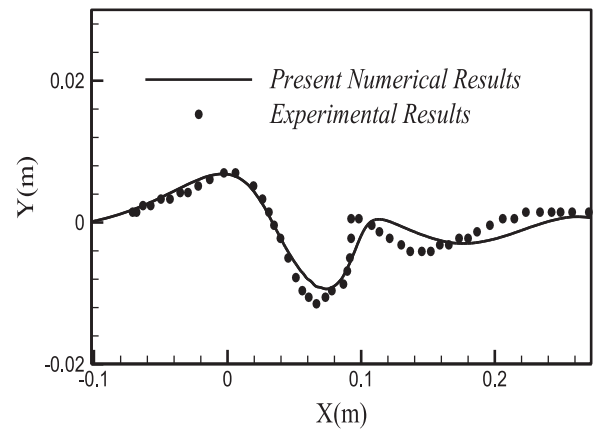


Fig. 7. Validation of free surface shape with experimental data of Cleaver et al. (2013).

Table 2

Geometrical parameters and flow condition of Cleaver et al. (2013) experimental study.

Re	40000
Free stream velocity	0.43 m/s
Submergence depth	C
Amplitude	0.2c
Chord length	0.1 m

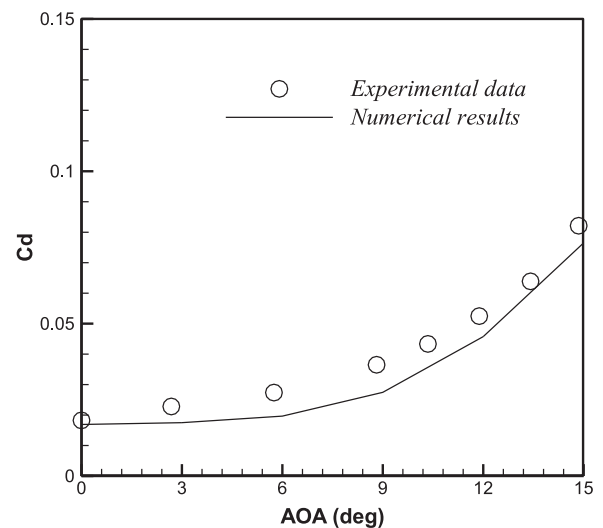


Fig. 8. comparison of numerical results of drag coefficient with experimental data of Custodio et al. (2015).

surface on the mean content of drag occurs in a range of critical frequencies and often in the unsteady parameter of 0.25. Additionally, the drag notably increases in this range. The more hydrofoil approaches the water surface, a vaster range of unsteady parameters is affected by the surface. In addition, the drag increment will be more sensible. At submergence depths of larger than c , the surface effect is only related to the critical unsteady parameter range. However, at $d = 0.5c$, drag increases significantly in the whole length of unsteady parameter and this effect will be maximum in the critical range. In order to design hydro-crafts which use hydrofoils to decrease drag, submergence depth should not be less than chord length. To predict the thrust force coefficient, the following relation was presented by Garrick (1937) in plunging motion.

$$C_T = \pi^3 Sr_A^2 (F^2 + G^2) \tag{8}$$

In this equation, F and G are the Theodorsen functions which are almost independent of frequency and $Sr_A = 2fa/U_0$ is Strouhal number

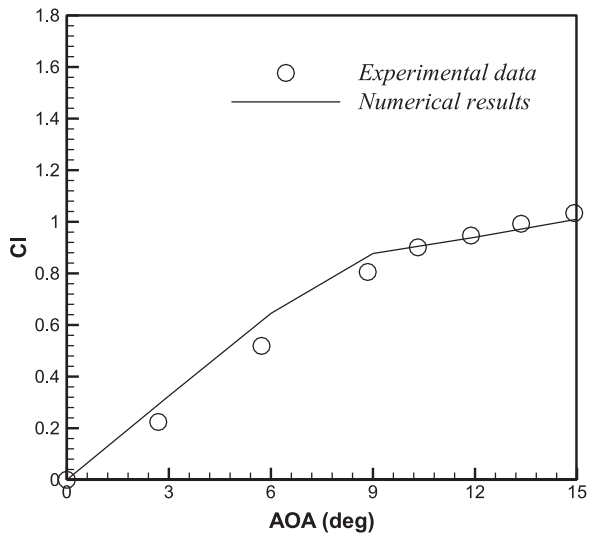


Fig. 9. comparison of numerical results of lift coefficient with experimental data of Custodio et al. (2015).

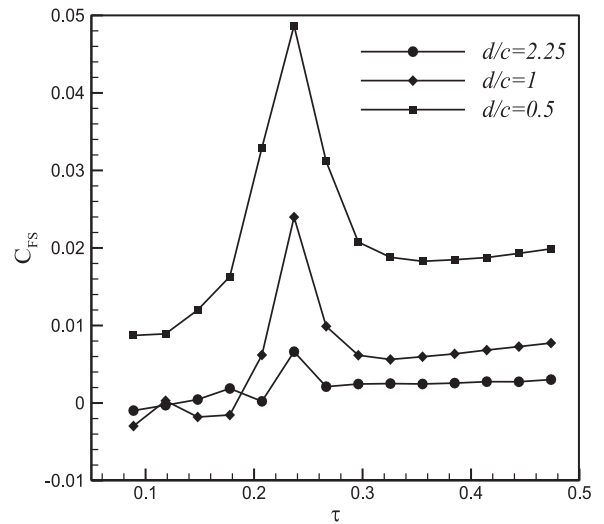


Fig. 12. Time-averaged drag coefficient due to free surface effect against unsteady parameter.

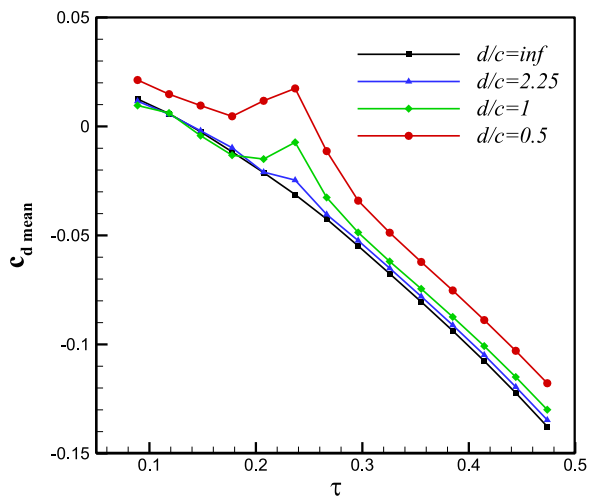


Fig. 10. Time-averaged drag coefficient against Strouhal number based on chord length.

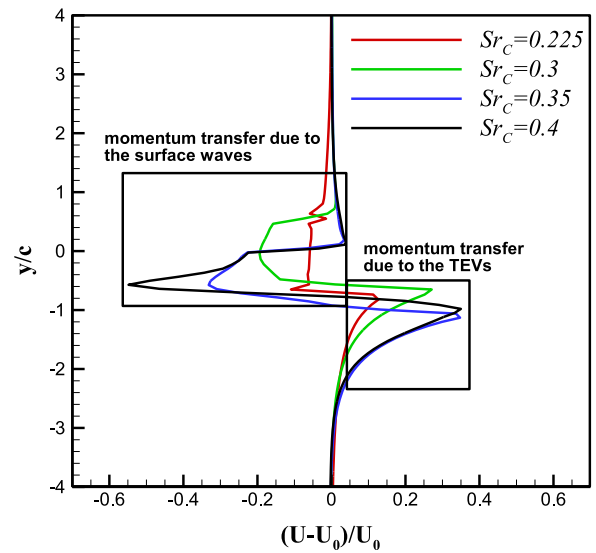


Fig. 13. Non-dimensional streamwise velocity profile at $t = 3T/4$ and $x/c = 2$.

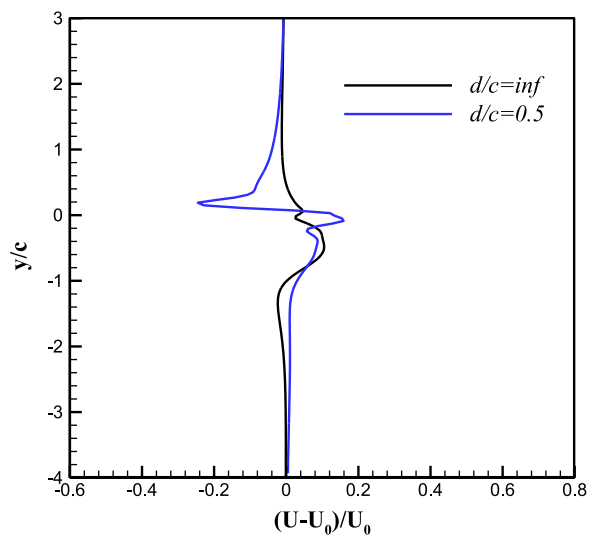


Fig. 11. Non-dimensional streamwise velocity profile at $Sr_c = 0.4$ and $x/c = 2$.

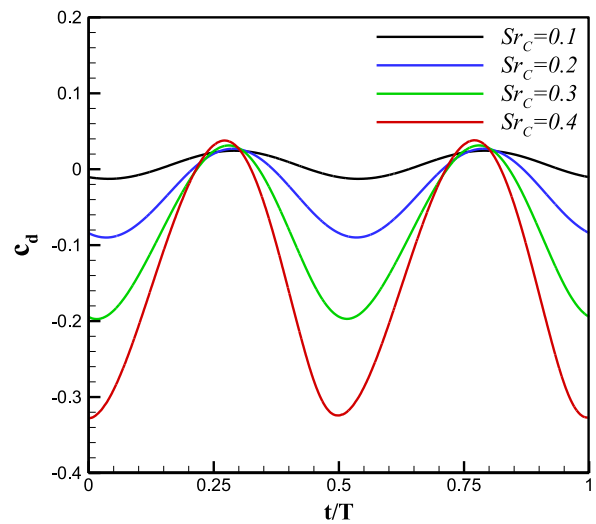


Fig. 14. Instantaneous drag coefficient at $d/c = inf..$

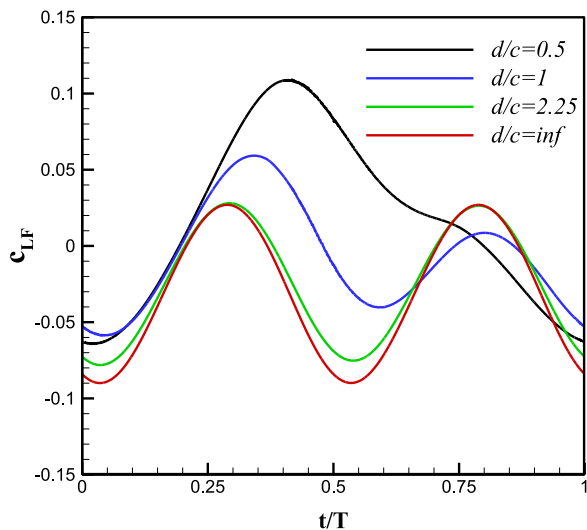


Fig. 15. Longitudinal force coefficient at $sr_c=0.2$.

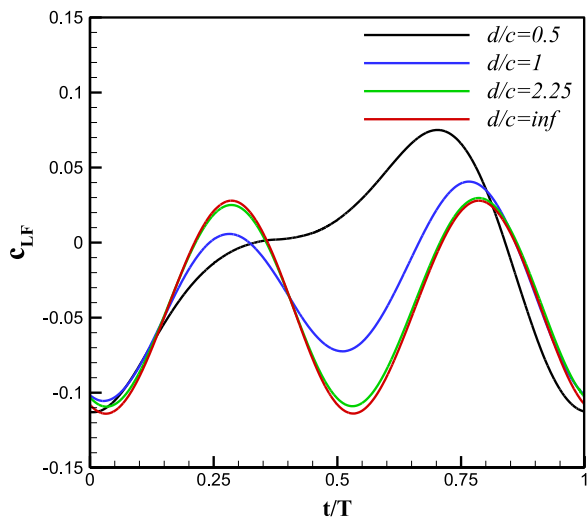


Fig. 16. Longitudinal force coefficient at $sr_c=0.225$.

based on amplitude. According to equation 8, the thrust force has a direct relation with the second exponent of Sr_A number. Thrust force coefficient can be computed properly by the above equation for the condition that there is no free surface impact and also for non-critical frequencies. However, when hydrofoil approaches the surface and in the critical frequency range, determination of drag is not possible by this equation.

In order to study the mechanism of production of thrust force and to understand the behavior of the forces efficiently, effective parameters of this force creation should be investigated separately. Produced horizontal force for an oscillating hydrofoil in the vicinity of the surface can be divided into three factors. The first one is friction drag which is always positive. This is the only mechanism to produce drag for a stationary hydrofoil at $d/c=inf$. The second one is the drag of mean transferred momentum which is developed by TEV of an oscillating hydrofoil and the last one is drag due to free surface effect. It should be noted that the mentioned factors can be affected by each other. For example, when the hydrofoil approaches the surface, the produced vortices at the trailing edge may be affected by the free surface. It seems that in large submergence depths and uncritical frequencies, the effects of free surface on strength and orientation of TEV are inconsiderable as shown by Cleaver et al. (2013). Thus, their mutual may be ignored. There is not any wave formation at $d/c=inf$. The drag due to free surface effect can be assessed by subtraction of

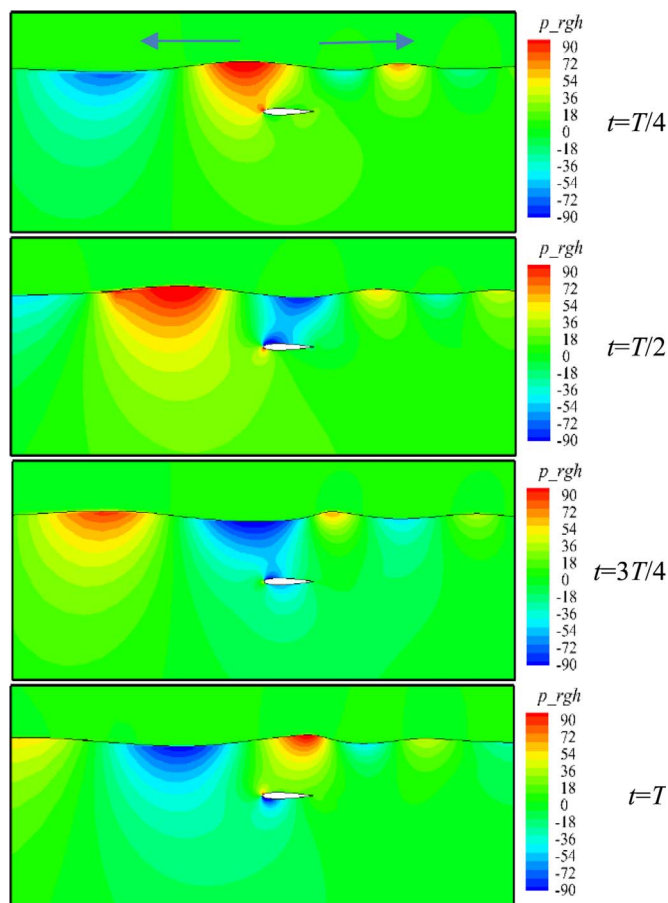


Fig. 17. Pressure contour around hydrofoil and free surface at $sr_c=0.2$ (upstream wave ← and downstream wave →).

temporal mean drag of the hydrofoil which is located near the free surface and one that is far enough from the surface for corresponding frequencies. The mentioned drag is determined by equation 9 as follow:

$$C_{FS}(d_o) = C_d(d_o) - C_d(d_\infty) \tag{9}$$

In this equation, d_o is an arbitrary submergence depth. Drag coefficient due to free surface effect based on the unsteady parameter is demonstrated in Fig. 12 for different submergence depths. It is found that this drag has a significant increase in the closer submergence depth and also in a range of critical unsteady parameters. Furthermore, this drag has an increasing trend by frequency enhancement even for supercritical conditions. This point implies the influence of hydrofoil oscillating frequency on drag. It can be deduced from Fig. 12 that large unsteady waves which are formed in this area are the main reason behind the drag increment in the critical frequency range. Larger waves transfer more contents of momentum and the drag increases due to their movement to downstream. In a range of supercritical frequencies, drag due to free surface effect increases by an increase in frequency since waves with larger amplitude are generated which transfer more momentum when the frequency is increased. In order to examine momentum transfer, streamwise velocity profile has been shown in the Fig. 13 for different frequencies in the downstream of the hydrofoil. Momentum deficit leads to drag, and momentum surplus leads to thrust (Jones et al., 1998). As shown in Fig. 13, momentum transfer due to surface waves participate in producing drag. By increasing frequency, the momentum transfer increases. Generally, drag increases when the hydrofoil approaches the water free surface. However, less drag is observed for $d/c = 1$ than $d/c = 2.25$ in subcritical frequencies according to Fig. 12. This is because the wave which moves upstream shifts momentum in order to decrease drag. This phenomenon is

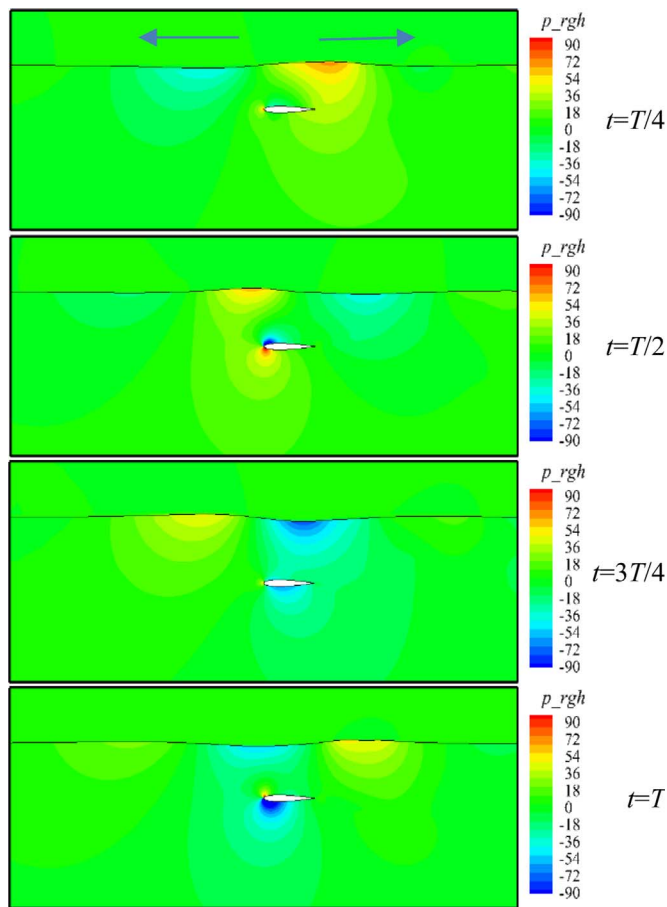


Fig. 18. Pressure contour around hydrofoil and free surface at $sr_c = 0.225$ (upstream wave ← and downstream wave →).

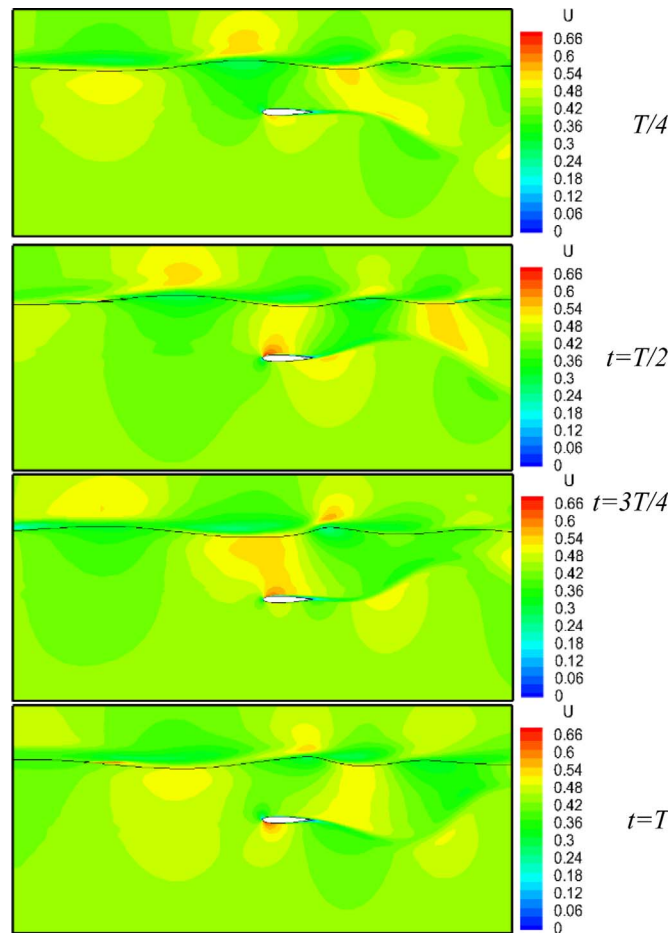


Fig. 19. Velocity contour around hydrofoil and free surface at $sr_c = 0.2$.

verified in the experimental result reported by Zhu et al. (2006).

Herein, the instantaneous behavior of force in a complete oscillation cycle is examined in order to study flow behavior properly. Instantaneous drag coefficient in the far field condition is investigated. Then the effect of submergence depth will be analyzed for subcritical and supercritical frequencies. Plunging velocity and subsequently thrust force have maximum value in the middle position for a complete cycle of plunging motion. While hydrofoil moves to the top position, plunging velocity and hence, thrust force decrease gradually until becoming zero at the top position as shown in Fig. 14. For all frequencies in the top and bottom positions where the plunging velocity is zero and independent of amplitude and frequency, the thrust force coefficient has almost the same value. Therefore, the flow field should be investigated in the middle position of the plunging motion for different frequencies for a better understanding of frequency impact on instantaneous thrust force and flow pattern. The other impact of frequency enhancement on instantaneous drag behavior is the creation of phase difference on the diagram. According to Fig. 12, the moment with maximum or minimum drag changes due to frequency alteration. In other words, the diagram of plunging motion and instantaneous drag has 90° phase difference at high frequencies while this difference is more than 90° for smaller frequencies.

Longitudinal force coefficient for a Strouhal number of 0.2 at different submergence depths is displayed in Fig. 15 for a complete oscillation cycle of the hydrofoil. It should be noted that Strouhal number of 0.2 is classified in the subcritical frequency range. There exist two peaks in this Figure which have the same size for $d/c = \infty$. However, by decreasing of submergence depth, the first peak gets larger while the second one is reduced to a minimum. In other words, peak sizes differ under the influence of free surface so that by

decreasing submergence depth, their difference will be more. In addition, the free surface has another impact on instantaneous drag behavior. At $d/c = \infty$, the first and second peak occur in $t = T/4$, which hydrofoil is located at the top position of plunging motion, and $t = 3T/4$, which hydrofoil is located at the bottom position, respectively. However, the first peak gets far from $t = T/4$ and approaches $t = T/2$ due to the hydrofoil approaching the surface. In addition, the existence of free surface causes a phase difference in the instantaneous drag diagram for different submergence depths. This procedure is reversed for supercritical frequencies. According to Fig. 16, there are also two peaks for $sr_c = 0.225$. However, the first and second peaks get smaller and larger as the submergence depth decreases. A comparison of the instantaneous drag coefficient at $d = 0.5c$, shows that the second peak fades away and the first one approaches $t = T/2$ for the subcritical condition and the reverse is true for the supercritical condition. So it seems that there is only one peak for drag in the critical unsteady parameter.

Dynamic pressure contours around the hydrofoil and the free surface are represented in Figs. 17 and 18 at subcritical and supercritical Strouhal number of 0.2 and 0.225, respectively. Each of the illustrations is plotted for $t = T/4, t = T/2, t = 3T/4$ and $t = T$.

Additionally, the free surface shape is displayed in these Figures. Low and high pressure regions are created at the free surface while wave camber is in downward and upward conditions, respectively. When the high and low pressure regions are in right and left hand sides of the hydrofoil, the force vector in the flow direction leads to drag decrement. However, it causes drag enhancement for the inverse condition.

According to this point, the inverse behavior of instantaneous drag coefficient is realizable in subcritical and supercritical frequencies. At

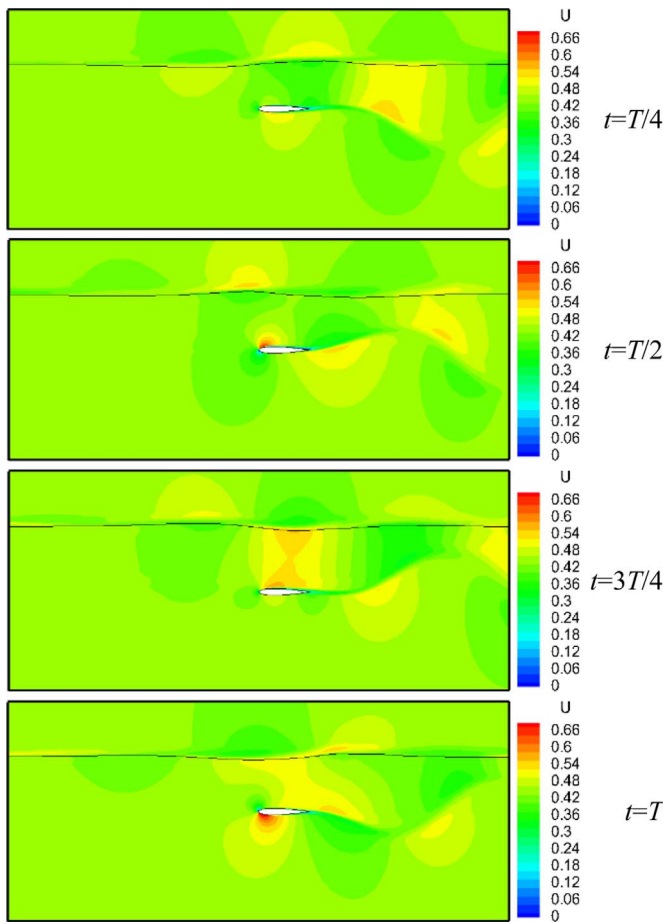


Fig. 20. Velocity contour around hydrofoil and free surface at $sr_c = 0.225$.

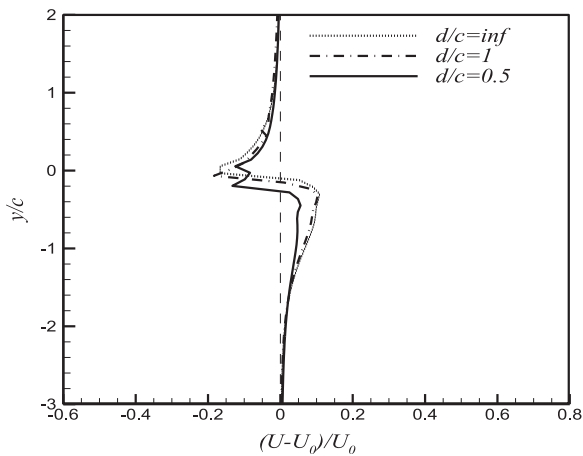


Fig. 21. Non-dimensional velocity profile at $sr_c = 0.3$, $t = T/2$ and $x/c = 2$.

subcritical Strouhal number of $Sr_c = 0.2$, the first peak is larger and its approximate location in the instantaneous drag diagram is at $t = T/4$. As seen in Fig. 17, the low and high pressure regions are in the right and left hand sides, respectively which lead to drag increment. The reverse procedure happens for the supercritical Sr_c of 0.225 (Fig. 18). According to Figs. 17 and 18, surface waves are moved to the upstream and downstream for subcritical frequencies. However, they are only moved to the downstream in supercritical frequencies.

Velocity contour for the subcritical Sr_c of 0.2 is demonstrated in Fig. 19. Hydrofoil is at the nearest distance from the surface at $t = T/4$. At this moment, all of the hydrofoil leading edge is surrounded by a low velocity area. This low velocity region moves to downstream in the next

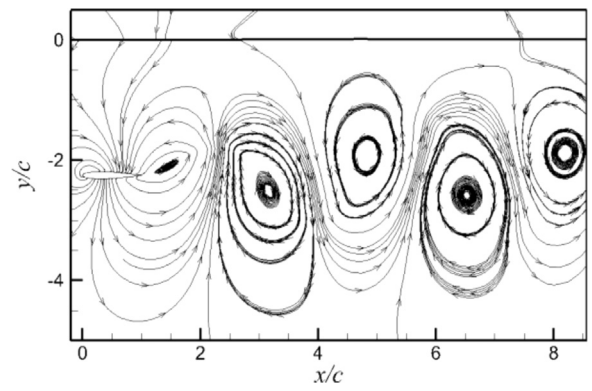


Fig. 22. Trailing edge vortices at $sr_c = 0.3$, $t = T/2$ and $d/c = 2.25$.

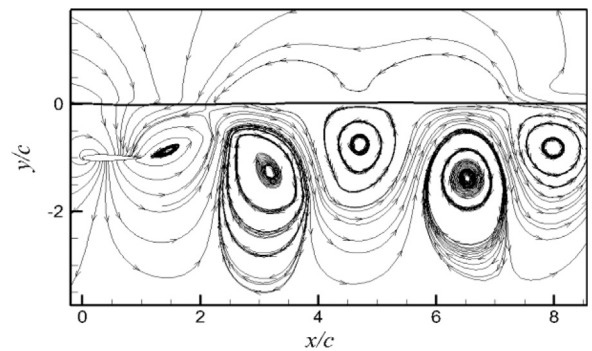


Fig. 23. Trailing edge vortices at $sr_c = 0.3$, $t = T/2$ and $d/c = 1$.

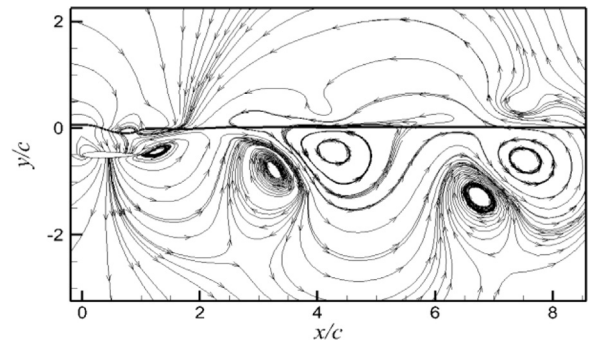


Fig. 24. Trailing edge vortices at $sr_c = 0.3$, $t = T/2$ and $d/c = 0.5$.

phase of the motion. Thus, the high velocity area is created in the upper zone of hydrofoil at $t = 3T/4$ when the hydrofoil is at the furthest distance from the surface. The velocity contour for supercritical Sr_c of 0.225 is shown in Fig. 20. Owing to the formation of smaller surface waves in this condition, the free surface has less impact on the flow field.

Dimensionless velocity profile for three different submergence depths is described in Fig. 21. The upper and lower deviations are related to surface waves and the transferred momentum of TEVs, respectively. The transferred momentum by vortices at $d = 2.25c$ and c are approximately the same. However, it is reduced for $d = 0.5c$ due to the impact of the free surface on TEVs and then on the transferred momentum. The mentioned vortices for the oscillating hydrofoil at $d = 2.25c$ are shown in Fig. 22. The surface impact on the drag coefficient is negligible and can be disregarded at this distance.

The lower and upper vortices are clockwise and counter-clockwise, respectively. Thus, there is a momentum surplus in Fig. 22 in order to increase the thrust force. Therefore, the formed vortices at the trailing edge are as producing thrust type. These vortices at the Sr_c number of 0.3 are described in Fig. 23 at $d = c$. The free surface does not have any effect on the existing vortices in this condition. However, they are

affected by the free surface in the other conditions.

The thrust force produced in the vortices pattern of von Karman Vortex Street depends on the vertical distance between the upper and lower vortices. In other words, the momentum increment of TEVs and the produced thrust force are reduced by decreasing this distance (Young, 2005). The vortices pattern for $d = 0.5c$ is represented in Fig. 24. By comparing with $d = 2.25c$ and c , the vortices releasing pattern changes due to the effect of free surface and also the vertical distance of the upper and lower vortices is reduced.

6. Conclusion

In this research study, the effects of the oscillation frequency and various submergence depths were investigated on oscillating hydrofoil drag. The N-S equations were solved in the vicinity of the water free surface in the critical unsteady parameter range. The main findings of the present study can be summarized as follows:

- The capability of the Navier-Stokes equations was verified for simulation of unsteady, viscous and turbulent flow around plunging hydrofoil in the vicinity of the free surface in comparison with experimental data.
- By comparing with experimental data, using N-S equations modified the infinity content problem of velocity potential function in the critical unsteady parameter.
- The mean content of the drag coefficient increases significantly in a range of critical unsteady parameters. This is due to the fact that large unsteady waves which are created in this zone shift more momentum in order to increase the drag.
- There are two peaks that are the same in the instantaneous drag diagram in the far field condition. The more submergence depth is reduced; the first and second peaks get larger and smaller, respectively at the subcritical Sr number. This procedure is reversed for supercritical condition.
- Due to the direction of the wave camber, surface eddy waves create low and high pressure regions at the free surface. Locating these regions on the left or right hand sides can cause an increment or decrement of drag.
- The free surface affects TEV and subsequently reduces transient momentum and thrust force for the critical frequency range and also for all frequencies of $d = 0.5c$. However, the free surface does not have any effect on TEV and transient momentum in the other conditions.

References

Ashraf, M.A., Young, J., S., Lai, J.C., 2012. Oscillation frequency and amplitude effects on plunging airfoil propulsion and flow periodicity. *AIAA J.* 50 (11), 2308–2324.

Bai, K.J., Han, J.H., 1994. A localized finite-element method for the nonlinear steady waves due to a two-dimensional hydrofoil. *J. ship Res.* 38 (1), 42–51.

Ceccio, S.L., 2010. Friction drag reduction of external flows with bubble and gas injection. *Annu. Rev. Fluid Mech.* 42 (1), 183–203.

Chung, M.-H., 2016. Propulsive performance of a flapping plate near a free surface. *J. Fluids Struct.* 65, 411–432.

Cleaver, D., Calderon, D.E., Wang, Z., Gursul, I., 2013. Periodically plunging foil near a free surface. *Exp. Fluids* 54 (3), 1–18.

Cleaver, D.J., Calderon, D.E., Wang, Z., Gursul, I., 2016. Lift enhancement through flexibility of plunging wings at low Reynolds numbers. *J. Fluids Struct.* 64, 27–45.

Cleaver, D.J., Gursul, I., Calderon, D.E., Wang, Z., 2014. Thrust enhancement due to flexible trailing-edge of plunging foils. *J. Fluids Struct.* 51, 401–412.

Custodio, D., Henoach, C., Johari, H., 2015. Aerodynamic characteristics of finite span wings with leading-edge protuberances. *AIAA J.* 53 (7), 1878–1893.

Dagan, G., Miloh, T., 1982. Free-surface flow past oscillating singularities at resonant frequency. *J. Fluid Mech.* 120, 139–154.

De Silva, L.W.A., Yamaguchi, H., 2012. Numerical study on active wave devouring propulsion. *J. Mar. Sci. Technol.* 17 (3), 261–275.

Djavareshkian, M.H., Esmaili, A., 2013. Neuro-fuzzy based approach for estimation of hydrofoil performance. *Ocean Eng.* 59, 1–8.

Djavareshkian, M.H., Esmaili, A., 2014. Heuristic optimization of submerged hydrofoil using ANFIS-PSO. *Ocean Eng.* 92, 55–63.

Djavareshkian, M.H., Esmaili, A., Parsania, A., 2013. Numerical simulation of smart hydrofoil in marine system. *Ocean Eng.* 73, 16–24.

Ducoin, A., Astolfi, J.A., Deniset, F., Sigrist, J.-F., 2009. Computational and experimental investigation of flow over a transient pitching hydrofoil. *Eur. J. Mech. - B/Fluids* 28 (6), 728–743.

Filippas, E.S., Belibassakis, K.A., 2014. Hydrodynamic analysis of flapping-foil thrusters operating beneath the free surface and in waves. *Eng. Anal. Bound. Elem.* 41, 47–59.

Forbes, L.K., 1985. A numerical method for non-linear flow about a submerged hydrofoil. *J. Eng. Math.* 19 (4), 329–339.

Garrick, I., 1937. Propulsion of a flapping and oscillating airfoil.

Gnoffo, P., 1982. A vectorized, finite-volume, adaptive grid algorithm applied to planetary entry problems, Proceedings of the 3rd Joint Thermophysics, Fluids, Plasma and Heat Transfer Conference, p. 1018.

Grue, J., Mo, A., Palm, E., 1988. Propulsion of a foil moving in water waves. *J. Fluid Mech.* 186, 393–417.

Haskind, M., 1954. On wave motion of a heavy fluid. *Prikl. Mat. Mekh* 18, 15–26.

Hirt, C.W., Nichols, B.D., 1981. Volume of fluid (VOF) method for the dynamics of free boundaries. *J. Comput. Phys.* 39 (1), 201–225.

Hough, G., Moran, S., 1969. Froude number effects on two-dimensional hydrofoils. *J. ship Res.* 13 (1), 53–60.

Jasak, H., 1996. Error Analysis and Estimation for the Finite Volume Method with Applications to Fluid Flows, 1996 (Ph. D. Thesis). University of London Imperial College.

Jones, K.D., Dohring, C.M., Platzer, M.F., 1998. Experimental and computational investigation of the Knoller-Betz effect. *AIAA J.* 36 (7), 1240–1246.

Kim, S.-H., Yamato, H., 2005. The estimation of wave elevation and wave disturbance caused by the wave orbital motion of a fully submerged hydrofoil craft. *J. Mar. Sci. Technol.* 10 (1), 22–31.

Kouh, J., Lin, T., Chau, S., 2002. Performance analysis of two-dimensional hydrofoil under free surface. *J. Natl. Taiwan Univ.* 86 (10), 113–123.

Landrini, M., Lugni, C., Bertram, V., 1999. Numerical simulation of the unsteady flow past a hydrofoil. *Ship Technol. Res.-Schiffstechnik* 46 (1), 14–30.

McCORMICK, M.E., Bhattacharyya, R., 1973. Drag reduction of a submersible hull by electrolysis. *Nav. Eng. J.* 85 (2), 11–16.

Menter, F.R., 1994. Two-equation eddy-viscosity turbulence models for engineering applications. *AIAA J.* 32 (8), 1598–1605.

Münch, C., Ausoni, P., Braun, O., Farhat, M., Avellan, F., 2010. Fluid–structure coupling for an oscillating hydrofoil. *J. Fluids Struct.* 26 (6), 1018–1033.

Palm, E., Grue, J., 1999. On the wave field due to a moving body performing oscillations in the vicinity of the critical frequency. *J. Eng. Math.* 35 (1–2), 219–232.

Plotkin, A., 1975. The thin-hydrofoil thickness problem including leading-edge corrections. *J. Ship Res.* 19, 2.

Prasad, B., Hino, T., Suzuki, K., 2015. Numerical simulation of free surface flows around shallowly submerged hydrofoil by OpenFOAM. *Ocean Eng.* 102, 87–94.

Shen, X., Ceccio, S.L., Perlin, M., 2006. Influence of bubble size on micro-bubble drag reduction. *Exp. Fluids* 41 (3), 415–424.

Winkel, E., Oweis, G., Vanapalli, S., Dowling, D., Perlin, M., Solomon, M., Ceccio, S., 2009. High-Reynolds-number turbulent boundary layer friction drag reduction from wall-injected polymer solutions. *J. Fluid Mech.* 621, 259–288.

Xie, N., Vassalos, D., 2007. Performance analysis of 3D hydrofoil under free surface. *Ocean Eng.* 34 (8), 1257–1264.

Xu, G.D., Meng, Q., 2016. Waves induced by a two-dimensional foil advancing in shallow water. *Eng. Anal. Bound. Elem.* 64, 150–157.

Xu, G.D., Wu, G.X., 2013. Hydrodynamics of a submerged hydrofoil advancing in waves. *Appl. Ocean Res.* 42, 70–78.

Young, J., 2005. Numerical Simulation of the Unsteady Aerodynamics of Flapping Airfoils. University of New South Wales, Australian Defence Force Academy, School of Aerospace, Civil and Mechanical Engineering.

Young, J., S., Lai, J.C., 2004. Oscillation frequency and amplitude effects on the wake of a plunging airfoil. *AIAA J.* 42 (10), 2042–2052.

Zanette, J., Imbault, D., Tourabi, A., 2010. A design methodology for cross flow water turbines. *Renew. Energy* 35 (5), 997–1009.

Zhu, Q., Liu, Y., Yue, D.K.P., 2006. Dynamics of a three-dimensional oscillating foil near the free surface. *AIAA J.* 44 (12), 2997–3009.